Am J Nucl Med Mol Imaging 2013;3(1):32-43
www.ajnmmi.us /ISSN:2160-8407/ajnmmi1209002

Original Article

A comparison of image contrast with ^{64}Cu-labeled long circulating liposomes and ^{18}F-FDG in a murine model of mammary carcinoma

Andrew W Wong, Eleanor Ormsby, Hua Zhang, Jai Woong Seo, Lisa M Mahakian, Charles F Caskey, Katherine W Ferrara

Department of Biomedical Engineering, University of California, Davis, CA 95616, USA

Received September 18, 2012; Accepted November 13, 2012; Epub January 5, 2013; Published January 15, 2013

Abstract: Conjugation of the ^{64}Cu PET radioisotope ($t_{1/2}$ = 12.7 hours) to long circulating liposomes enables long term liposome tracking. To evaluate the potential clinical utility of this radiotracer in diagnosis and therapeutic guidance, we compare image contrast, tumor volume, and biodistribution of ^{64}Cu-liposomes to metrics obtained with the dominant clinical tracer, ^{18}F-FDG. Twenty four female FVB mice with MET1 mammary carcinoma tumor grafts were examined. First, serial PET images were obtained with the ^{18}F-FDG radiotracer at 0.5 hours after injection and with the ^{64}Cu-liposome radiotracer at 6, 18, 24, and 48 hours after injection (n = 8). Next, paired imaging and histology were obtained at four time points: 0.5 hours after ^{18}F-FDG injection and 6, 24, and 48 hours after ^{64}Cu-liposome injection (n = 16). Tissue biodistribution was assessed with gamma counting following necropsy and tumors were paraffin embedded, sectioned, and stained with hematoxylin and eosin. The contrast ratio of images obtained using ^{18}F-FDG was 0.88 ± 0.01 (0.5 hours after injection), whereas with the ^{64}Cu-liposome radiotracer the contrast ratio was 0.78 ± 0.01, 0.89 ± 0.01, 0.88 ± 0.01, and 0.94 ± 0.01 at 6, 18, 24, and 48 hours, respectively. Estimates of tumor diameter were comparable between ^{64}Cu-liposomes and ^{18}F-FDG, ^{64}Cu-liposomes and necropsy, and ^{64}Cu-liposomes and ultrasound with Pearson's r-squared values of 0.79, 0.79, and 0.80, respectively. Heterogeneity of tumor tracer uptake was observed with both tracers, correlating with regions of necrosis on histology. The average tumor volume of 0.41 ± 0.05 cc measured with ^{64}Cu-liposomes was larger than that estimated with ^{18}F-FDG (0.28 ± 0.04 cc), with this difference apparently resulting primarily from accumulation of the radiolabeled particles in the pro-angiogenic tumor rim. The imaging of radiolabeled nanoparticles can facilitate tumor detection, identification of tumor margins, therapeutic evaluation and interventional guidance.

Keywords: ^{64}Cu, ^{18}F-FDG, liposomes, mammary carcinoma, PET, preclinical, biodistribution

Introduction

Liposomes passively accumulate in tumors due to the enhanced permeability and retention effect of leaky vasculature and dysfunctional lymphatics [1]. This effect has been used to enhance drug delivery [2], but can also generate contrast for imaging and detection of tumors. While classic contrast agents are expected to readily clear from the body, pegylated liposomes have a long blood circulation half-life [3]. Early liposomal radiolabeling efforts made use of ^{18}F ($t_{1/2}$ = 109.8 minutes), which allowed liposomes to be tracked for a few hours [4, 5]. Conjugation with ^{64}Cu ($t_{1/2}$ = 12.7 hours) allows liposomes to be tracked over several days [6]. Use of a radioisotope with a half-life comparable to liposome kinetics enhances the contrast generated from tumor accumulation and blood clearance of liposomes, while avoiding additional radioactive hazards associated with longer lived isotopes [6, 7]. Enhanced contrast may improve high-sensitivity detection and tracking of tumors that display enhanced permeability and retention of nanoparticles, as well as the ability to use imaging to predict therapeutic response to liposomal drug formulations. In addition, the long lived radioisotope expands the practical window for diagnostic imaging as well as facilitating PET-guided inter-

ventions such as radiation therapy, where ^{18}F-FDG images are used in treatment planning [8], or surgery, where ^{18}F-FDG and handheld gamma probes are used to localize tumors [9, 10].

Labeling of liposomes with ^{64}Cu is enabled by advances in radioisotope metal chelation chemistry. Requirements include stable chelation *in vitro* and *in vivo*, fast, gentle labeling, and minimal purification of labeled nanoparticles. 6-[*p*-(bromoacetamido)benzyl]-1,4,8,11-tetraazacyclotetradecane-*N,N',N'',N'''*-tetraacetic acid (BAT)-PEG1.2k-lipid (BAT-PEG-lipid) containing liposomes fulfill each of these requirements. BAT is a highly stable copper chelator, demonstrating excellent stability when conjugated to ^{67}Cu in serum over five days [11]. We have previously demonstrated the stability of BAT in ^{64}Cu-liposomes, where incubation of ^{64}Cu-liposomes with mouse serum at 37°C revealed that 6 % of radioactivity transferred to serum after 20 hours, and 8 % transferred to serum after 48 hours, as measured by thin layer chromatography [6]. Attachment of BAT to a pegylated lipid enables production of liposomes that can be quickly and gently labeled and require minimal purification [6]. Gentle chelation conditions are important to liposome labeling, as high chelation temperatures can disrupt many liposome formulations. Although 4,11-bis(carboxymethyl)-1,4,8,11-tetraazabicyclo[6.6.2]hexadecane (CB-TE2A) has been shown to chelate ^{64}Cu with great stability, in a liposomal labeling system, the high temperature required for chelation can affect liposomal stability. In addition, direct comparisons of the blood radioactivity using BAT and CB-TE2A to track liposomes have demonstrated that the blood circulation of the radiolabeled particle is very similar [12], consistent with previous studies of radiolabeled antibodies [13].

^{18}F-FDG acts as a glucose analogue approximating cellular metabolism. It is ideal for imaging because it is not metabolized but rather phosphorylated and trapped within cells, and also rapidly clears from the bloodstream [14], leading to a stable imaging window and high image contrast. Furthermore, as high glucose utilization is typical of cancerous cells, it is broadly applicable in cancer imaging. However, inflammation and infection may also lead to high ^{18}F-FDG uptake [15], potentially confounding cancer imaging. Further, not all tumors are metabolically active [16], and many normal tissues display high uptake of ^{18}F-FDG [17], modulated by disease states such as diabetes [18] or physical exertion before and during scanning. These factors complicate interpretation of ^{18}F-FDG PET imaging and help to motivate the development of novel imaging tracers.

There are many ways to measure tracer uptake and tumor volume in an ^{18}F-FDG scan. Options to measure metabolic activity include nonlinear kinetic analysis [19], simplified kinetic models [20], and corrected standardized uptake value (SUV) [21]. Nonlinear kinetic analysis is the gold standard of metabolic activity measurement with PET. This method makes use of a three compartment pharmacokinetic model, driven by ^{18}F-FDG region of interest (ROI) analysis of tumors and the aortic input function. Unfortunately, measurement of the aortic input function requires long dynamic scans or repeated arterial blood sampling, rendering the gold standard clinically impractical. The simplified kinetic model requires a single venous blood sample, using population average parameters and the venous blood sample to calculate the input function. SUV is the ratio of the tracer in the region of interest to the injected dose of tracer. This method is the simplest and most commonly clinically used. Various correction factors for patient physiology are used to allow for better approximation of metabolic uptake, including bodyweight, body surface area, and blood sugar. It will be important to choose the appropriate image quantitation metrics to compare the utility of ^{18}F-FDG and ^{64}Cu-liposomes.

The MET1 mammary carcinoma model is a syngeneic mouse model of breast cancer. These tumor cells express polyoma virus middle T, a molecular mimic of human Her2/neu, commonly overexpressed in human breast cancer [22]. Both genes induce oncogenesis through the Shc and PI-3 kinase pathways [23]. MET1 mammary carcinomas are histopathologically similar to high grade human breast cancer; they form solid tumors with central necrosis, are locally invasive, highly mitotic, with adenocarcinomatous gland formation [24]. MET1 mammary carcinoma serves as a good model of human primary breast cancer.

To further assess the utility of radiolabeled nanoparticles, we perform a comparison of

images generated with ^{18}F-FDG and ^{64}Cu-liposomes. We hypothesize that ^{64}Cu-liposomes can serve as effective tumor contrast agents in the murine MET1 mammary carcinoma model. We examine image quality, biodistribution, tumor delivery, tumor heterogeneity, and tumor size estimation.

Methods and materials

Solvents and other reagents were purchased from Sigma-Aldrich unless otherwise noted. Lipids and a liposome mini-extruder were purchased from Avanti Polar Lipids. BAT-PEG-lipid conjugate was synthesized by Fmoc solid phase synthesis as previously described [6]. $^{64}CuCl_2$ was purchased from Washington University in St. Louis (MO) while ^{18}F-FDG was purchased from PETNET Solutions (San Diego, CA) under a protocol controlled by the University of California, Davis. Dulbecco's Phosphate Buffered Saline (DPBS) was purchased from Invitrogen Corporation (Carlsbad, CA).

Preparation of ^{64}Cu-liposomes

The ^{64}Cu-liposome labeling procedure followed a previously reported method [6]. In brief, lipids in chloroform (0.555/0.39/0.05/0.005 mol/mol/mol/mol, hydrogenated soy phosphatidylcholine (HSPC), cholesterol, 1,2-distearoyl-*sn*-glycero-3-phosphoethanolamine-*N*-[methoxy(polyethylene glycol)-2000] (DSPE-PEG2k-OMe), BAT-PEG-lipid) were transferred to a test tube and solvent evaporated under nitrogen. After overnight lyophilization, lipids were suspended in 0.1 M ammonium citrate solution (400 µL, 300 mOsm, pH 5.5), and incubated in a warm bath (60°C) alternating with gentle vortexing for 10 minutes. The lipid mixture was extruded through a 100 nm membrane filter (Whatman, NJ) at 60°C. After cooling to room temperature, buffered $^{64}CuCl_2$ (18.5 MBq/mg lipid) in 0.1 M ammonium citrate (pH 5.5, 0.1 ml) was added to the extruded lipid solution. The mixture was incubated at 30°C for 40 minutes, then 0.1 M ethylenediaminetetraacetic acid in deionized water (20 µL) was added and incubated for an additional 10 minutes. ^{64}Cu-liposomes and unbound copper were separated by size exclusion chromatography with Sephadex G75 resin (GE Healthcare) in DPBS. A portion of ^{64}Cu-liposomes were retained until the radioactivity decayed, nanoparticle size was then measured by Dynamic Light Scattering performed with a Nicomp 380 ZLS (Particle Sizing Systems, CA).

In vivo study design

All animal studies were approved by the University of California, Davis Animal Care and Use Committee (**Figure 1**). A total of 24 female FVB mice were examined (6-10 weeks old, 15-25 g, Charles River, MA). During procedures, mice were anesthetized, induced with 3.5 % isoflurane and maintained with 2.0 - 2.5 % isoflurane. Syngeneic MET1 mammary carcinomas [24] were transplanted into the mammary fat pad of the first cohort of eight mice 13 days prior to injection, and the second cohort of sixteen mice were transplanted 21 days prior. Mice in the first cohort underwent PET scanning 0.5 hours after injection with ^{18}F-FDG, waited 4 hours, and then were injected with ^{64}Cu-liposomes. Mice were then imaged at 6, 18, 24 and 48 hours, and sacrificed for necropsy and biodistribution. Mice in the second cohort underwent ultrasound imaging 12 hours prior to ^{18}F-FDG injection, were imaged 0.5 hours after injection, and then after a wait period of 4 hours were injected with ^{64}Cu-liposomes and imaged at 6, 24, and 48 hours following liposome injection. Subgroups of four mice were sacrificed for necropsy, biodistribution, and histological sections after each imaging time point.

Ultrasound imaging

Mice were depilated with hair clippers and Veet® cream. Tumors were imaged with a Siemens Sequoia ultrasound system (Siemens Preclinical Solutions). Tumors were sized by hand segmentation of elliptical regions of interest on transverse and sagittal images, and tumor volume was then estimated from the diameters of an ellipsoid assuming rotational symmetry about the major diameter.

PET imaging

Mice were injected with 500 MBq/kg ^{18}F-FDG via tail vein and imaged after 0.5 hours of rest. All PET imaging was performed with two mice side by side for 0.5 hours, using a microPET Focus 120 scanner (Siemens Preclinical Solutions). Four hours after completion of ^{18}F-FDG imaging, mice were injected with 1 mg of

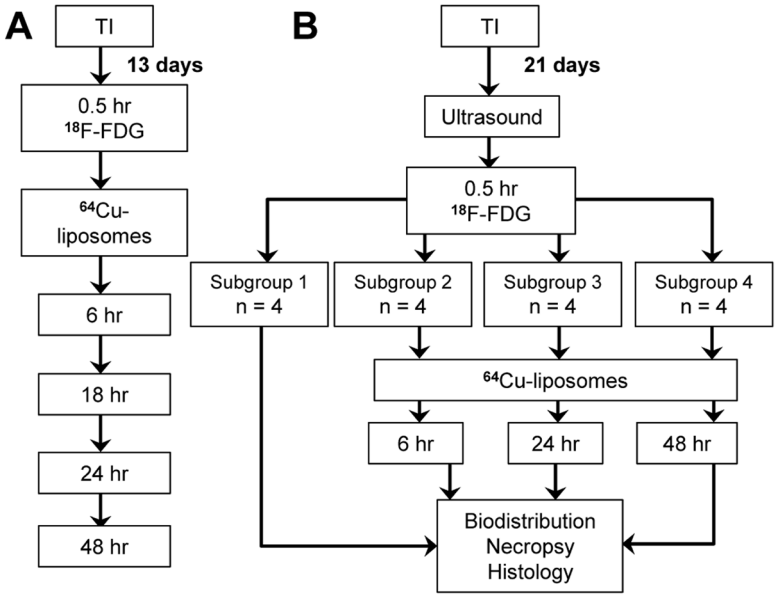

Figure 1. Study design diagram. A: The first cohort (n = 8 mice) was imaged 13 days after tumor implantation. Images were first acquired with ^{18}F-FDG 0.5 hours after injection. Mice were then injected with ^{64}Cu-liposomes and imaged at 6, 18, 24, and 48 hours after injection. B: The second cohort (n = 16 mice) was imaged 21 days after tumor implantation with ultrasound and then with ^{18}F-FDG at 0.5 hours after injection. Subgroups of 4 mice were then sacrificed at each imaging time point: 0.5 hours after ^{18}F-FDG injection (without PET imaging), 6, 24, and 48 hours after ^{64}Cu-liposome injection (with ^{18}F-FDG and ^{64}Cu-liposome PET imaging). TI = Tumor Implantation.

^{64}Cu-liposomes (300 and 600 MBq/kg), and imaged for 0.5 hours at each time point following injection. PET Images were reconstructed with maximum a posteriori algorithm and tumors manually segmented by a single blinded observer with ImageJ (National Institutes of Health) and ASIPro software (Siemens Preclinical Solutions). ^{64}Cu-liposome PET tumor volumes were modeled by subtraction of a 0.8 mm spherical shell from ROI. Activity measured within 3D volumes was time-decay corrected and expressed as percent injected dose per cc of tissue (%ID/cc). Contrast ratios were calculated as in **Equation 1** [25], with values expressed as %ID/cc and averaged across subjects. Heterogeneity was calculated as the sum of the absolute value of the difference between individual pixels and the ROI average value over the ROI average value in %ID/cc (**Equation 2**), and averaged across subjects. This metric captures the variability in tracer uptake within a tumor.

Equation 1:

$$Contrast\ Ratio = \frac{tumor_{max} - muscle_{mean}}{tumor_{max} + muscle_{mean}}$$

Equation 2

$$Heterogeneity = \sum_{ROI} \left| \frac{pixel - mean}{mean} \right|$$

Necropsy and biodistribution

Following imaging, mice were euthanized by cervical dislocation, their organs removed, weighed, and radioactivity measured by Wizard 1470 Automatic Gamma Counter (Perkin Elmer). Tumors were formalin fixed overnight and then paraffin embedded, sectioned, and stained with hematoxylin and eosin. Tumor size was estimated by measuring the long axis and the longest perpendicular distance of a paraffin section and then modeling the tumor as a sphere with diameter given by the average of the two measured distances.

Results

Characterization of ^{64}Cu-liposomes

Liposomes measured 120 ± 13.6 nm in diameter. Decay corrected labeling yield was greater than 95% by radioactive thin layer chromatography.

PET image analysis

PET images of a mouse obtained after injection with ^{18}F-FDG or ^{64}Cu-liposomes are displayed in **Figure 2**. ^{64}Cu-liposomes label the blood pool, strongly enhancing the heart, jugular veins, and liver at 6 hours after injection. The outline of tumors is also visible. After 18 hours, radioactivity appears in the intestines and bladder, and tumors are more strongly labeled. At 24 hours after injection, the strength of the signal from the heart, jugular veins, and liver has fallen, although tumor activity is equivalent to that observed at 18 hours. At 48 hours after injec-

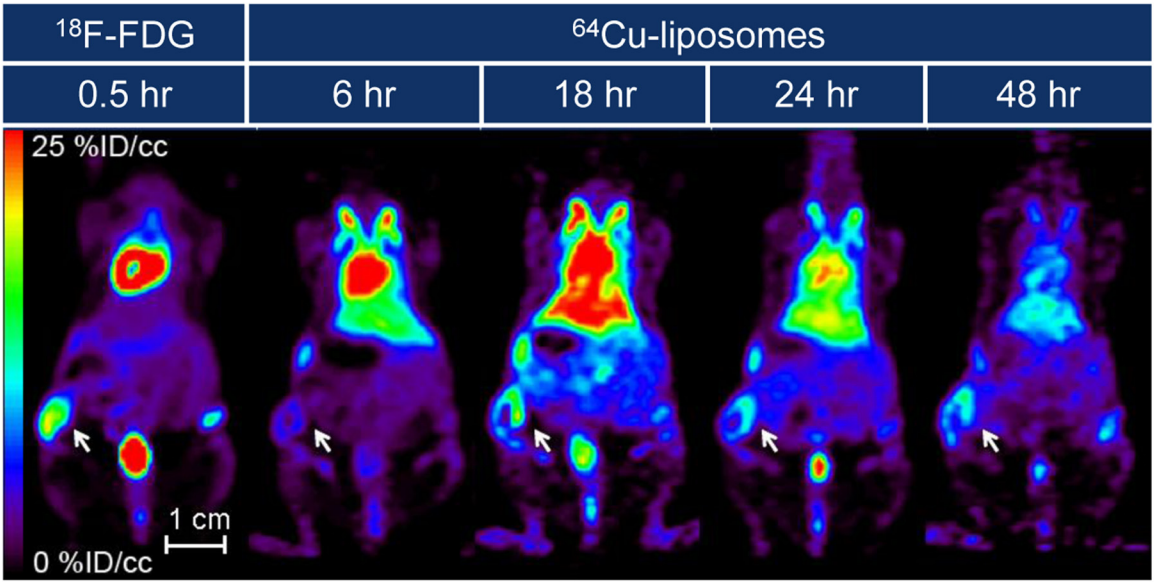

Figure 2. In a mouse from the cohort imaged 13 days after tumor implantation, PET images obtained 0.5 hours after injection with ^{18}F-FDG are compared with images obtained 6, 18, 24, and 48 hours after injection with the ^{64}Cu-liposome tracer. ^{64}Cu-liposome accumulation in tumors (arrows) increased from 6 to 18 hours and then remained consistent through 48 hours while background activity decreased.

Table 1. *In Vivo* Tumor Accumulation and Contrast Ratio, ^{18}F-FDG and ^{64}Cu-liposomes, cohort imaged 13 days after tumor implantation. All values are reported as mean ± standard error of the mean (SEM) (n = 16 tumors)

Tracer	Time point	PET Tumor Volume (cc)	Contrast Ratio	Average Tumor Accumulation (%ID/cc)	Total Tumor Accumulation (%ID)
^{18}F-FDG	0.5 hr	0.12 ± 0.01	0.88 ± 0.01	5.7 ± 0.3	0.7 ± 0.1
^{64}Cu-liposomes	6 hr	0.04 ± 0.01	0.78 ± 0.01	3.7 ± 0.1	0.4 ± 0.1
^{64}Cu-liposomes	18 hr	0.09 ± 0.01	0.89 ± 0.01	7.6 ± 0.3	1.5 ± 0.1
^{64}Cu-liposomes	24 hr	0.08 ± 0.01	0.88 ± 0.01	6.0 ± 0.2	1.1 ± 0.1
^{64}Cu-liposomes	48 hr	0.09 ± 0.01	0.94 ± 0.01	5.9 ± 0.2	1.1 ± 0.1

tion, the tumor accumulation remains high while other areas continue to lose signal, the blood activity is reduced, and intestines are no longer distinguishable from surrounding tissues. In the cohort of mice injected 13 days after tumor implantation, tumor accumulation peaks at 18 hours (**Table 1**). In the second cohort, injected with the radiotracer 21 days after implantation, extravasation increases over 48 hours while total tumor activity falls over 48 hours (**Table 2**) due to the decrease in blood activity. In both cohorts, ^{64}Cu-liposome accumulation was greater than that of ^{18}F-FDG, at later time points, where ^{64}Cu-liposome accumulation exceeded ^{18}F-FDG accumulation from 18 to 48 hours (**Figure 3**). Distribution of contrast within the tumor was heterogeneous, with regions of contrast hypointensity correlating with necrosis as demonstrated by hematoxylin and eosin (**Figure 4**). Evaluation of heterogeneity reveals that in the first cohort (with smaller tumors), heterogeneity is comparable amongst all categories except that it is less in ^{64}Cu-liposome images at 6 hours. In the second cohort (with larger tumors), all ^{64}Cu-liposome images demonstrate greater heterogeneity than those obtained with ^{18}F-FDG (**Figure 5**).

Biodistribution

Ex vivo gamma counting of organs demonstrates that liposomes remain in circulation

Table 2. *Ex Vivo* and *In Vivo* Tumor Accumulation, ^{18}F-FDG and ^{64}Cu-liposomes, cohort imaged 21 days after tumor implantation. Subgroup 1 did not undergo PET imaging as mice were sacrificed 0.5 hour after ^{18}F-FDG injection. All values are reported as mean ± SEM (n = 8 tumors). Values are average %ID/cc, with total tumor %ID in parenthesis

	Subgroup 1	Subgroup 2	Subgroup 3	Subgroup 4
Accumulation based on ^{18}F-FDG ROI		5.5±0.1 (2.0±0.4)	5.0±0.3 (1.5±0.4)	4.9±0.2 (0.9±0.2)
Time of measurement		0.5 hr	0.5 hr	0.5 hr
Accumulation based on ^{64}Cu-liposome ROI		5.3 ± 0.3 (2.1 ± 0.4)	8.8 ± 0.3 (4.3 ± 1.0)	9.9 ± 0.6 (3.5 ± 0.7)
Time of measurement		6 hr	24 hr	48 hr
Necropsy Derived	7.8 ± 0.4 (3.0 ± 0.6)	7.6±0.9 (2.1±0.3)	12.1 ± 1.1 (2.9 ± 0.7)	18.9 ± 1.2 (3.0 ± 0.6)
Time of measurement	0.5 hr	6 hr	24 hr	48 hr

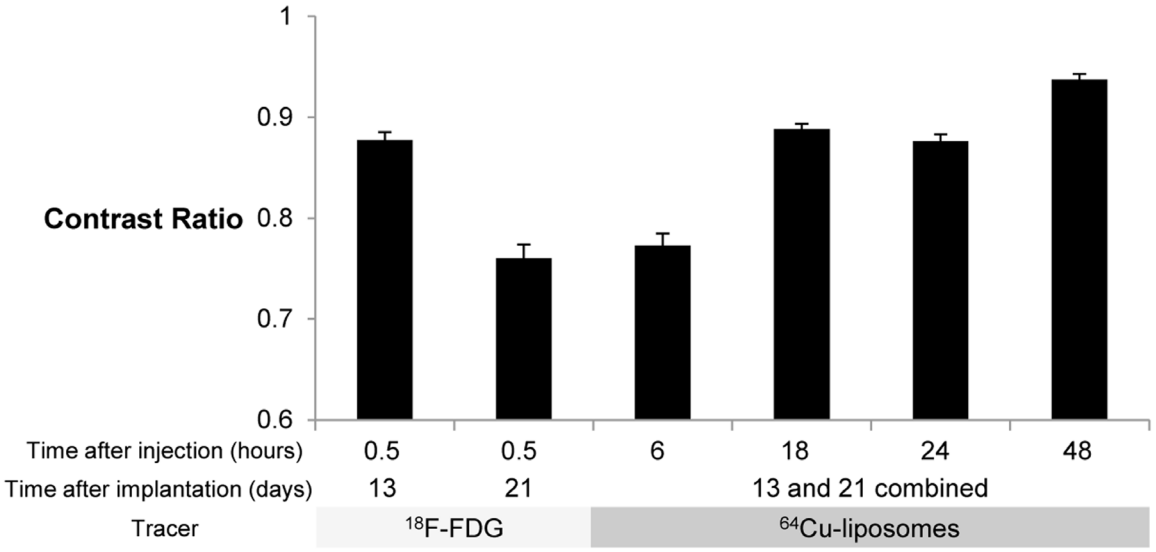

Figure 3. Contrast Ratio comparison with ^{18}F-FDG and ^{64}Cu-liposome tracers. Contrast ratio was defined as ($Tumor_{Max}$ – $Muscle_{Mean}$) / ($Tumor_{Max}$ + $Muscle_{Mean}$) in %ID/cc. Error bars represent SEM. For mice imaged with ^{18}F-FDG 13 days after implantation and mice imaged 18 hours after injection with ^{64}Cu-liposomes, n = 16 tumors, for all other groups, n = 24 tumors. Cohort imaged 13 days after implantation was maintained under anesthesia for the period between injection of ^{18}F-FDG and imaging, while mice imaged 21 days after implantation were awakened between injection of ^{18}F-FDG and imaging, resulting in a reduction in the contrast ratio. For the mice that remained under anesthesia during ^{18}F-FDG image acquisition (13 days after implantation), at the earliest time point, the contrast ratio is higher for images obtained with ^{18}F-FDG than ^{64}Cu-liposomes, but is comparable at the 18 and 24 hour time points. At 48 hours after injection of ^{64}Cu-liposomes, tumor contrast ratio was in all cases superior to ^{18}F-FDG images.

over 48 hours, with 6.1 ± 0.3 %ID/g still present within the blood pool after 48 hours (**Table 4**). Tumor radioactivity assessed *ex vivo* confirmed image derived trends, although absolute values assessed by *ex vivo* methods are larger likely due to attenuation and differing ROI selection as compared with surgical margins. Selection of surrounding, lower intensity tissue depresses tumor average intensity relative to dissection values. At all time points liposomes demonstrated lower accumulation in heart, muscle, and brain compared to ^{18}F-FDG. The brain received 6.9 ± 0.6 %ID/g of ^{18}F-FDG versus 0.8 ± 0.0 %ID/g of ^{64}Cu-liposomes. Murine *ex vivo* FDG distribution after 1 hour demonstrated high uptake in the urine and heart, with 98.5 ±

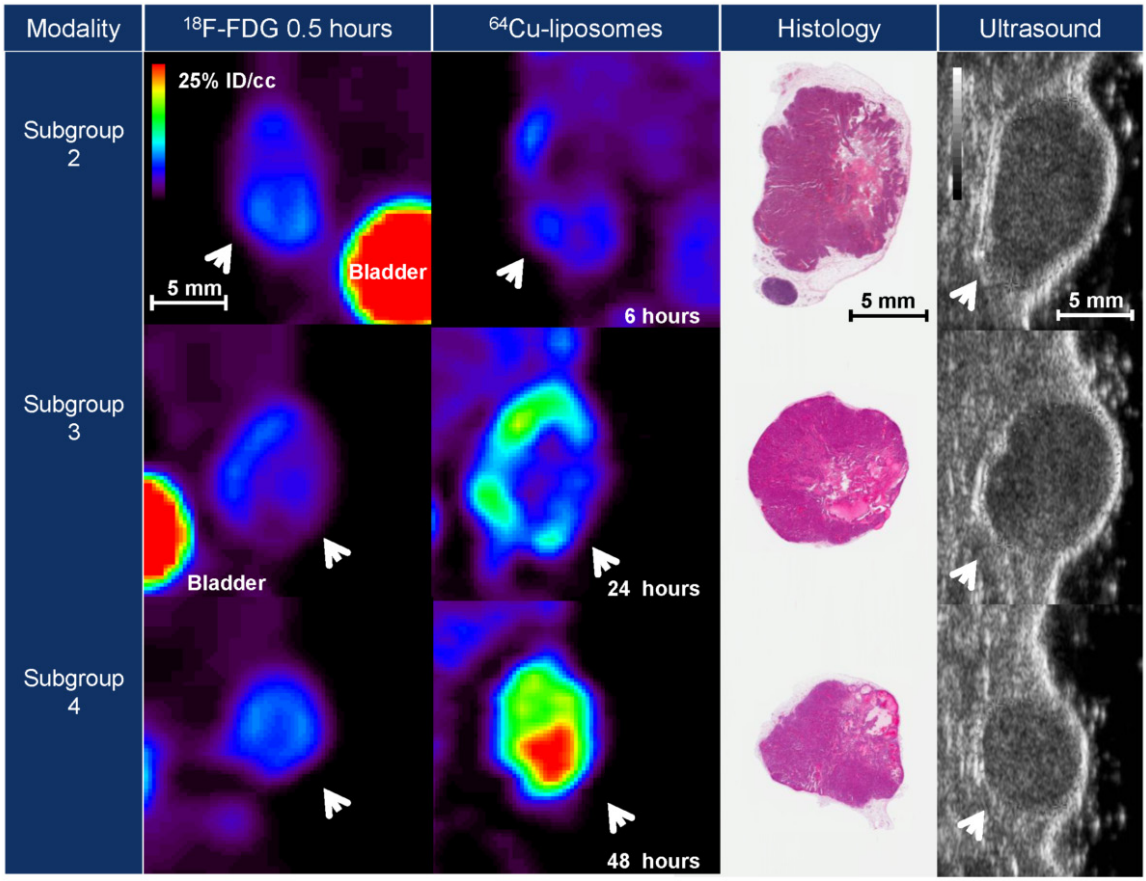

Figure 4. Typical images resulting from ^{18}F-FDG and ^{64}Cu-liposome PET tracers, histopathology and ultrasound. Images are representative of subgroups 2-4 (as described in Figure 1) acquired 21 days after tumor implantation. Tumor volume is comparable with ^{18}F-FDG and ^{64}Cu-liposome tracers. In addition, hypointense regions observed with both PET tracers correlate to regions of necrosis as determined by hematoxylin and eosin staining.

2.2 and 51.2 ± 6 %ID/g respectively. High uptake of both tracers was evident in tumor as well with 7.8 ± 0.4 %ID/g of ^{18}F-FDG compared to 12.1 ± 1.1 and 18.9 ± 1.2 %ID/g of ^{64}Cu-liposomes detected in the tumor after 24 and 48 hours, respectively.

Tumor size estimation

Tumor size was evaluated with ultrasound, necropsy weight, and histological sections as well as ^{18}F-FDG and ^{64}Cu-liposome PET ROI analysis (**Table 3**). Images from three tumors from different time points imaged by multiple methods are presented in **Figure 4**. Images from each agent and modality display gross morphological similarities. Tumor volume correlated strongly with each modality, and the slopes of linear regression analysis were near 1 (**Figure 6**).

Discussion

There are many methods to measure tracer uptake and tumor volume in an ^{18}F-FDG scan. Functional measures of permeability cannot be directly compared against functional measures of metabolic activity. Here, we chose to use an uncorrected SUV, expressed as percentage of initial dose per mass of tissue (%ID/g), as a simple measure of uptake which is directly applicable to both tracers. For comparison of image quality, however, a simple comparison of SUV ignores the normal background distribution of ^{18}F-FDG [17] and liposomes. Calculation of the contrast ratio includes correction for background, facilitating comparison of local uptake. We found that the contrast ratio for the ^{64}Cu-liposome radiotracer was equivalent to or greater than that obtained with ^{18}F-FDG at most time points.

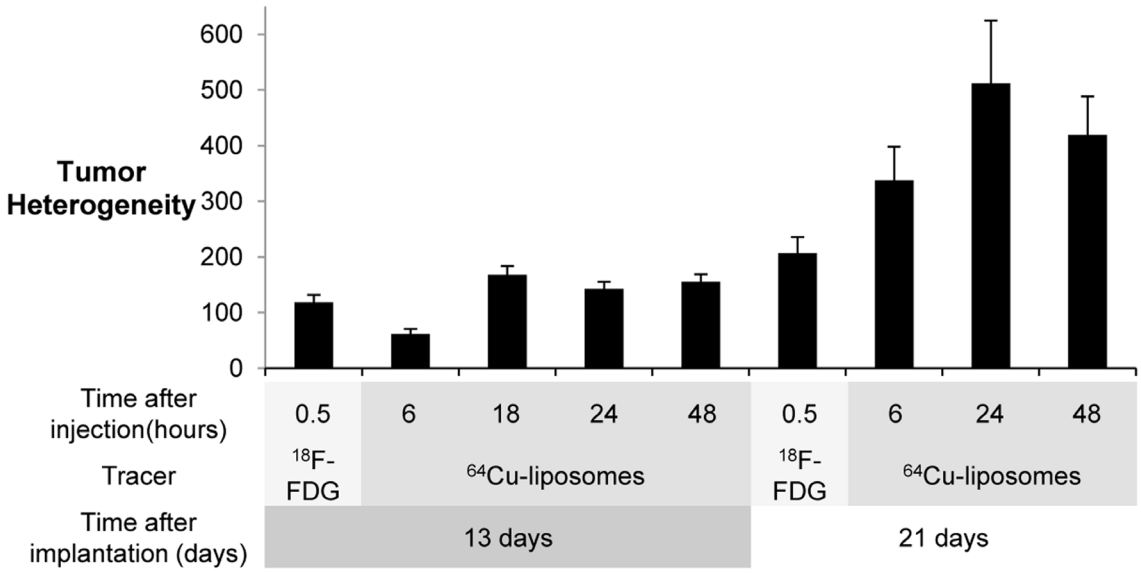

Figure 5. Tumor Heterogeneity, as observed with ^{18}F-FDG and ^{64}Cu-liposome PET tracers, for cohorts imaged 13 and 21 days after tumor implantation. Heterogeneity was defined as sum of absolute value in %ID/cc of (pixel - ROI_{mean}) / ROI_{mean} (Equation 2) with error bars representing SEM. N = 16 tumors for the cohort of mice imaged 13 days after implantation, n = 8 tumors for the cohort of mice imaged 21 days after implantation. Heterogeneity of images obtained with ^{64}Cu-liposomes is less than that obtained with ^{18}F-FDG at 6 hours in the cohort imaged 13 days after implantation, but is greater in all other groups.

Table 3. Tumor Volume, cohort imaged 21 days after tumor implantation. Tumor volume is reported as mean ± SEM, with tumor volume measured in cc (n = 8 tumors). ^{64}Cu-liposome volume includes correction by subtraction of spherical shell

Method	Subgroup 2	Subgroup 3	Subgroup 4
^{64}Cu-liposomes	0.25 ± 0.06	0.29 ± 0.07	0.18 ± 0.04
Necropsy	0.32 ± 0.06	0.26 ± 0.06	0.16 ± 0.03
Ultrasound	0.22 ± 0.05	0.15 ± 0.04	0.08 ± 0.02
^{18}F-FDG	0.37 ± 0.08	0.29 ± 0.07	0.18 ± 0.03
Histology	0.16 ± 0.05	0.17 ± 0.06	0.06 ± 0.02

Upon administration, ^{64}Cu-liposomes distribute within the blood pool, and are slowly trapped by tumors and the reticuloendothelial system. The liver and spleen process and excrete the nanoparticles, clearing the blood pool over 48 hours. When mice are imaged at 6 hours, a high blood concentration of ^{64}Cu-liposomes, 41.9 ± 1.3 %ID/cc, reduces the tumor contrast ratio. However, at later time points, hepatic excretion of liposomes reduces blood concentration, improving background. In addition, tumors continue to accumulate the tracer over 48 hours, with serial images demonstrating increases from 0.7 ± 0.1 to 1.1 ± 0.1 %ID/cc. This effect could not be observed with previous radiolabeling methods using ^{18}F, however, the longer half-life of ^{64}Cu enables tumor visualization with a high tumor/background contrast ratio over 48 hours. This extended tumor image contrast could be used for tumor detection, but also for direct measurement of nanoparticle accumulation, individual prediction of therapeutic efficacy, or in guidance of therapeutic intervention.

There are many clinical methods of quantitating tumor size with PET, including tumor volume directly measured from region of interest segmentation, the product of the greatest perpendicular dimensions of tumors (WHO) or the longest tumor dimension on transaxial images (RECIST) [26]. Comparing imaging studies

Table 4. Ex Vivo Biodistribution, ^{18}F-FDG and ^{64}Cu-liposomes, cohort imaged 21 days after tumor implantation. All values are reported as mean ± SEM (n = 8 for tumors and kidneys, n = 4 all other organs)

%ID/g					%ID			
Group	Subgroup 2	Subgroup 3	Subgroup 3	Subgroup 4	Subgroup 1	Subgroup 2	Subgroup 3	Subgroup 4
Tracer	^{18}F-FDG	^{64}Cu-liposomes			^{18}F-FDG	^{64}Cu-liposomes		
Time point	0.5 hr	6 hr	24 hr	48 hr	0.5 hr	6 hr	24 hr	48 hr
Blood	1.8 ± 0.3	41.9 ± 1.3	19.1 ± 1.7	6.1 ± 0.3	-	-	-	-
Urine	98.5 ± 2.2	1.4 ± 0.3	5.3 ± 0.8	1.9 ± 0.4	-	-	-	-
Spleen	3.1 ± 0.4	18.2 ± 2.3	19.2 ± 1.1	12.5 ± 0.7	0.4 ± 0.1	1.8 ± 0.2	1.6 ± 0.2	1.0 ± 0.0
Lungs	4.5 ± 0.3	8.5 ± 0.6	5.1 ± 0.4	3.4 ± 0.1	0.7 ± 0.0	1.2 ± 0.1	0.9 ± 0.2	0.5 ± 0.0
Diaphragm	5.7 ± 1.6	4.8 ± 0.7	3.4 ± 0.6	1.6 ± 0.1	0.4 ± 0.0	0.3 ± 0.1	0.2 ± 0.0	0.1 ± 0.0
Heart	51.2 ± 6.1	4.8 ± 0.5	4.1 ± 0.3	2.5 ± 0.3	5.9 ± 0.6	0.5 ± 0.1	0.5 ± 0.0	0.3 ± 0.0
Liver	2.0 ± 0.3	9.4 ± 3.1	13.8 ± 0.5	7.2 ± 0.4	2.4 ± 0.3	10.6 ± 3.6	14.4 ± 0.3	7.6 ± 0.2
Kidneys	4.7 ± 0.3	8.6 ± 0.6	7.4 ± 0.2	6.1 ± 0.2	0.7 ± 0.0	1.2 ± 0.1	1.1 ± 0.1	0.9 ± 0.0
Duodenum	2.7 ± 0.3	3.9 ± 0.3	6.7 ± 0.3	5.3 ± 0.2	-	-	-	-
Jejunum	3.0 ± 0.4	3.3 ± 0.2	5.4 ± 0.1	4.9 ± 0.5	-	-	-	-
Quadriceps	2.2 ± 0.3	0.8 ± 0.1	1.2 ± 0.2	0.6 ± 0.1	-	-	-	-
Fat pad	1.5 ± 0.2	2.0 ± 0.3	1.5 ± 0.3	1.0 ± 0.1	-	-	-	-
Brain	6.9 ± 0.6	0.8 ± 0.0	0.4 ± 0.0	0.2 ± 0.0	2.8 ± 0.3	0.3 ± 0.0	0.2 ± 0.0	0.1 ± 0.0
Bone	2.0 ± 0.2	2.4 ± 0.3	2.6 ± 0.3	1.7 ± 0.1	-	-	-	-
Tumors	7.8 ± 0.4	7.6 ± 0.9	12.1 ± 1.1	18.9 ± 1.2	3.0 ± 0.6	2.1 ± 0.3	2.9 ± 0.7	3.0 ± 0.6

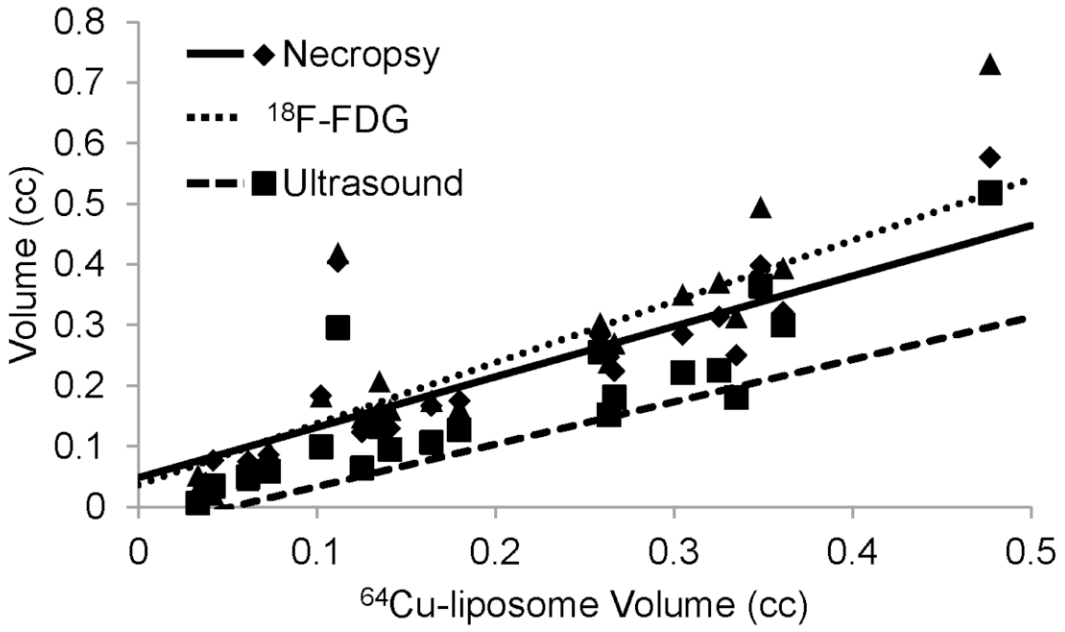

Necropsy	y = 0.833x + 0.048, R^2 = 0.79
^{18}F-FDG	y = 1.008x + 0.036, R^2 = 0.79
Ultrasound	y = 0.760x + 0.012, R^2 = 0.80

Figure 6. Correlation between tumor volumes determined with ^{64}Cu-liposome PET images, necropsy, ^{18}F-FDG PET images, and ultrasound in cohort of mice imaged 21 days after tumor implantation (n = 24 tumors). Each technique demonstrates strong correlation and comparable slope.

obtained with ^{18}F-FDG and ^{64}Cu-liposomes in a preclinical model of mammary carcinoma allows for the measurement of tumor volume by necropsy and weight in addition to PET, ultra-

sound, and histologic approaches. Then, comparison to the gold standard of weight on necropsy is most easily accomplished with tumor volume as opposed to one or two dimensional metrics. The quantitative image metrics of SUV, contrast ratio, and tumor volume facilitate comparison between ^{18}F-FDG and ^{64}Cu-liposomes.

As nanoparticle accumulation has a different physiological basis than ^{18}F-FDG accumulation, it is important to examine the comparative estimates of tumor volume. Five methods were used to estimate tumor size, with strong correlation between all five methods. As the raw average tumor diameter measured with ^{64}Cu-liposomes was ~1.3 mm larger than that estimated by ^{18}F-FDG, ^{64}Cu-liposome based size estimates were modified to include the subtraction of a 0.8 mm spherical shell from the tumor, bringing ^{64}Cu-liposome image derived size estimates in line with ^{18}F-FDG image derived size estimates. Comparison of PET images suggests that ^{64}Cu-liposomes are accumulating in a rim about the tumor (as compared with ^{18}F-FDG which did not concentrate in this region), most likely due to angiogenesis and tumor expansion. With this accumulation near the tumor margin in combination with the positron range effect, the tumor diameter is expected to be larger with the ^{64}Cu-liposome tracer. The correction resulted in close equivalence of linear regression for necropsy weight, ^{18}F-FDG, and ^{64}Cu-liposomes. Growth of tumor over the 48 hour study period, as well as the hypothesis that enhanced permeability extends beyond the metabolically active part of the tumor may also contribute to this difference in diameter. Tumor growth is not sufficient to explain this effect, as the average tumor size of the subgroup sacrificed at 48 hours was less than that of the previous subgroups. The ability to easily identify the angiogenic rim with ^{64}Cu-liposomes is intriguing for surgical resection and external beam radiation, where it may serve as a rational, imaging driven margin for excision.

We also utilized these radiotracers to image tumor heterogeneity. MET1 tumors demonstrate central necrosis and cystic regions which appear on ^{18}F-FDG PET as hypointense regions which may be caused by necrosis or inhibition of tumor metabolism. ^{64}Cu-liposome imaging produces similar patterns of hypointensity (**Figure 4**), which may be due to loss of vascular supply to cystic and necrotic regions, visible in histological sections. While ^{18}F-FDG, a small molecule, may easily diffuse through the extracellular space, ^{64}Cu-liposomes, with an average diameter of 120 nm, extravasate at a slower rate than small molecules. This correlation may be useful for assessment of therapeutic response, in which ^{64}Cu-liposomes would be administered as a physiologic imaging tracer of necrosis. In addition, ^{64}Cu-liposome images demonstrate a higher degree of heterogeneity as compared to ^{18}F-FDG (**Figure 5**). This heterogeneity results from the long circulating half-life of ^{64}Cu-liposomes (**Table 4**) and preferential accumulation of nanoparticles in regions of high vascular flow and permeability. In the tumors imaged 13 days after tumor implantation, at 6 hours after injection of the tracer, the difference between hypointense and hyperintense regions of the tumor is less than that of ^{18}F-FDG, but as nanoparticles continue to gather in the tumor, the contrast between regions of high and low uptake is greater than that of metabolic differences shown with ^{18}F-FDG. In the more nanoparticle-avid tumors from the cohort of mice imaged 21 days after implantation, ^{64}Cu-liposomes demonstrate greater heterogeneity at all time points. Thus, ^{64}Cu-liposomes are potential contrast agents for the assessment of nanoparticle delivery and vascular heterogeneity, with contrast advantages relative to ^{18}F-FDG.

Conclusion

This study compared tumor images generated by ^{64}Cu-liposomes with images generated by the dominant clinical tracer, ^{18}F-FDG. Inclusion of this standard provides a method to compare our proposed contrast agent against the clinical standard in our animal model of mammary carcinoma. A multiplicity of methods for calculating tumor dose and size were used and corroborated, including image derived tumor accumulation and size, ultrasound and histological size estimates, as well as tumor radioactivity and tumor weight following necropsy. A limitation of the study was that the tumors had to be imaged sequentially with two tracers as opposed to simultaneously and therefore variations in growth patterns can influence results. Another limitation is that the MET1 tumor model involves implantation of a tumor into a

known location and therefore observers were aware of the tumor location. This study demonstrates that in the mouse tumor model, ^{64}Cu-liposomes generate images with contrast and volume estimates comparable to ^{18}F-FDG. ^{64}Cu labeling facilitates liposomal tracking, has a mechanism of tumor uptake unique from that of ^{18}F-FDG, and we find that ^{64}Cu-liposomes may serve as a useful clinical contrast agent for detection of tumors, delineation of margins, prediction of therapeutic response, determination of therapeutic efficacy, and interventional guidance.

Acknowledgments

This work was supported by the National Cancer Institute, NIH RO1 CA 103828 NIH RO1 CA134659, and Radiological Society of North America Resident Research Grant RR0811.

Conflict of interest statement

The authors declare that they have no conflict of interest.

Address correspondence to: Dr. Katherine W Ferrara, Department of Biomedical Engineering, University of California, Davis, 451 Health Sciences Drive, Davis, California 95616, USA. Phone: (530) 7549436; Fax: (530) 7545739; E-mail: kwferrar@ucdavis.edu

References

[1] Maeda H. The enhanced permeability and retention (EPR) effect in tumor vasculature: the key role of tumor-selective macromolecular drug targeting. Adv Enzyme Regul 2001; 41: 189-207.

[2] Northfelt DW, Dezube BJ, Thommes JA, Miller BJ, Fischl MA, Friedman-Kien A, Kaplan LD, Du Mond C, Mamelok RD and Henry DH. Pegylated-liposomal doxorubicin versus doxorubicin, bleomycin, and vincristine in the treatment of AIDS-related Kaposi's sarcoma: results of a randomized phase III clinical trial. J Clinical Oncol 1998; 16: 2445-2451.

[3] Klibanov AL, Maruyama K, Torchilin VP and Huang L. Amphipathic polyethyleneglycols effectively prolong the circulation time of liposomes. FEBS Lett 1990; 268: 235-237.

[4] Oku N, Tokudome Y, Tsukada H and Okada S. Real-time analysis of liposomal trafficking in tumor-bearing mice by use of positron emission tomography. Biochim Biophys Acta 1995; 1238: 86-90.

[5] Marik J, Tartis MS, Zhang H, Fung JY, Kheirolomoom A, Sutcliffe JL and Ferrara KW. Long-circulating liposomes radiolabeled with [^{18}F]fluorodipalmitin ([^{18}F]FDP). Nucl Med Biol 2007; 34: 165-171.

[6] Seo JW, Zhang H, Kukis DL, Meares CF and Ferrara KW. A Novel Method to Label Preformed Liposomes with ^{64}Cu Positron Emission Tomography (PET) Imaging. Bioconjug Chem 2008; 19: 2577-2584.

[7] Petersen AL, Binderup T, Rasmussen P, Henriksen JR, Elema DR, Kjær A and Andresen TL. ^{64}Cu loaded liposomes as positron emission tomography imaging agents. Biomaterials 2011; 32: 2334-2341.

[8] Ford EC, Herman J, Yorke E and Wahl RL. ^{18}F-FDG PET/CT for Image-Guided and Intensity-Modulated Radiotherapy. J Nucl Med 2009; 50: 1655-1665.

[9] Piert M, Burian M, Meisetschlager G, Stein HJ, Ziegler S, Nahrig J, Picchio M, Buck A, Siewert JR and Schwaiger M. Positron detection for the intraoperative localisation of cancer deposits. Eur J Nucl Med Mol Imaging 2007; 34: 1534-1544.

[10] Kim WW, Kim JS, Hur SM, Kim SH, Lee SK, Choi JH, Kim S, Choi JY, Lee JE, Kim JH, Nam SJ, Yang JH and Choe JH. Radioguided surgery using an intraoperative PET probe for tumor localization and verification of complete resection in differentiated thyroid cancer: a pilot study. Surgery 2011; 149: 416-424.

[11] Moi MK, Meares CF, Mccall MJ, Cole WC and Denardo SJ. Copper-Chelates as Probes of Biological-Systems - Stable Copper-Complexes with a Macrocyclic Bifunctional Chelating Agent. Anal Biochem 1985; 148: 249-253.

[12] Seo JW, Mahakian LM, Kheirolomoom A, Zhang H, Meares CF, Ferdani R, Anderson CJ and Ferrara KW. Liposomal Cu-64 Labeling Method Using Bifunctional Chelators: Poly(ethylene glycol) Spacer and Chelator Effects. Bioconjug Chem 2010; 21: 1206-1215.

[13] Kukis DL, Li M and Meares CF. Selectivity of Antibody-Chelate Conjugates for Binding Copper in the Presence of Competing Metals. Inorg Chem 1993; 32: 3981-3982.

[14] Gallagher BM, Ansari A, Atkins H, Casella V, Christman DR, Fowler JS, Ido T, MacGregor RR, Som P, Wan CN, Wolf AP, Kuhl DE and Reivich M. Radiopharmaceuticals XXVII. ^{18}F-labeled 2-deoxy-2-fluoro-d-glucose as a radiopharmaceutical for measuring regional myocardial glucose metabolism in vivo: tissue distribution and imaging studies in animals. J Nucl Med 1977; 18: 990-996.

[15] Mochizuki T, Tsukamoto E, Kuge Y, Kanegae K, Zhao S, Hikosaka K, Hosokawa M, Kohanawa M and Tamaki N. FDG uptake and glucose

transporter subtype expressions in experimental tumor and inflammation models. J Nucl Med 2001; 42: 1551-1555.
[16] Cook GJ, Houston S, Rubens R, Maisey MN and Fogelman I. Detection of bone metastases in breast cancer by ^{18}FDG PET: differing metabolic activity in osteoblastic and osteolytic lesions. J Clinical Oncol 1998; 16: 3375-3379.
[17] Nakamoto Y, Tatsumi M, Hammoud D, Cohade C, Osman MM and Wahl RL. Normal FDG distribution patterns in the head and neck: PET/CT evaluation. Radiology 2005; 234: 879-885.
[18] Diederichs CG, Staib L, Glatting G, Beger HG and Reske SN. FDG PET: elevated plasma glucose reduces both uptake and detection rate of pancreatic malignancies. J Nucl Med 1998; 39: 1030-1033.
[19] Phelps ME, Huang SC, Hoffman EJ, Selin C, Sokoloff L and Kuhl DE. Tomographic Measurement of Local Cerebral Glucose Metabolic-Rate in Humans with (F-18)2-Fluoro-2-Deoxy-D-Glucose - Validation of Method. Ann Neurol 1979; 6: 371-388.
[20] Hunter GJ, Hamberg LM, Alpert NM, Choi NC and Fischman AJ. Simplified measurement of deoxyglucose utilization rate. J Nucl Med 1996; 37: 950-955.
[21] Huang SC. Anatomy of SUV. Nucl Med Biol 2000; 27: 643-646.
[22] Ross J and Fletcher J. The HER-2/neu Oncogene in Breast Cancer: Prognostic Factor, Predictive Factor, and Target for Therapy. Oncologist 1998; 3: 237-252.
[23] Webster MA, Hutchinson JN, Rauh MJ, Muthuswamy SK, Anton M, Tortorice CG, Cardiff RD, Graham FL, Hassell JA and Muller WJ. Requirement for both Shc and phosphatidylinositol 3' kinase signaling pathways in polyomavirus middle T-mediated mammary tumorigenesis. Mol Cell Biol 1998; 18: 2344-2359.
[24] Borowsky AD, Namba R, Young LJ, Hunter KW, Hodgson JG, Tepper CG, McGoldrick ET, Muller WJ, Cardiff RD and Gregg JP. Syngeneic mouse mammary carcinoma cell lines: two closely related cell lines with divergent metastatic behavior. Clin Exp Metastasis 2005; 22: 47-59.
[25] Nomori H, Watanabe K, Ohtsuka T, Naruke T, Suemasu K and Uno K. Evaluation of F-18 fluorodeoxyglucose (FDG) PET scanning for pulmonary nodules less than 3 cm in diameter, with special reference to the CT images. Lung Cancer 2004; 45: 19-27.
[26] Wahl RL, Jacene H, Kasamon Y and Lodge MA. From RECIST to PERCIST: Evolving Considerations for PET response criteria in solid tumors. J Nucl Med 2009; 50 Suppl 1: 122S-150S.